CrossMark

# Fire Experiments and Simulations in a Full-Scale Atrium Under Transient and Asymmetric Venting Conditions

*P. Ayala\* and A. Cantizano, Instituto de Investigación Tecnológica, Escuela Técnica Superior de Ingeniería, Universidad Pontificia Comillas, C/ Santa Cruz de Marcenado 26, 28015 Madrid, Spain*

*G. Rein, Department of Mechanical Engineering, Imperial College London, London, UK*

*G. Vigne, JVVA Fire Safety Consultants, Madrid, Spain*

*C. Gutiérrez-Montes, Fluid Dynamics Division of the Department of Mining and Mechanical Engineering, Universidad de Jaén, Jaén, Spain*

**Abstract.** An experimental and numerical comparison of new full-scale atrium fire tests in the 20 m cubic atrium with four different heat release rates (1.7 MW, 2.3 MW, 3.9 MW and 5.3 MW) is presented. Different exhaust conditions (steady and transient extraction rates) and different make-up air configurations (symmetric and asymmetric) are assessed. Temperature measurements in the near (fire plume) and far field (close to the walls) have been recorded by means of 59 thermocouples. The smoke layer interface is also estimated by means of a thermocouple tree with 28 measurements using the least-square and the n-percent methods. The simulations have been conducted using FDS (version 6, Release Candidate 3). The comparison with the simulations shows average discrepancies lower than 32% and 11%, for the near and far field temperatures, respectively. A discrepancy lower than 5% (1 m) is obtained by both methods for the smoke layer height when the steady state is reached. Finally, a slower response to an increment on the exhaust rate is predicted on the smoke layer, being more perceptible for high heat release rates.

## 1. Introduction

Nowadays, new architectural trends lead to fire safety designs supported by computational fluid dynamics (CFD) simulations, due to the applicability limits of the fire safety regulations. They are usually used to predict fire dynamics and smoke movement, fire dynamic simulator (FDS) [1] being the most used. In the case of atria, the smoke behaviour and its management constitutes one of the major concerns in fire safety designs, and then in CFD simulations. The accurate evaluation of the smoke layer can be translated into large amount of savings and lives. In

---

\* Correspondence should be addressed to: P. Ayala, E-mail: pablo.ayala@iit.upcomillas.es

this context, the smoke layer interface plays an important role, and the study of the different parameters and conditions that affect it is a key issue. Four of the most important parameters that influence the smoke layer interface are the HRR, the smoke production, the exhaust conditions and the make-up air supply [2]. However, these models should be validated for the different fire-induced conditions, the full-scale fire tests being a valuable source to be used as a benchmark, even more considering the high investment needed and the difficulties to build up a suitable test facility, which lead to a scarcity of full-scale fire data tests.

On this matter, atrium full-scale fire tests were carried out with heat release rates (HRR) up to 5 MW in China by Chow et al. [3] and in Canada by Lougheed et al. [4]. Additionally, Gutierrez et al. [5–8] validated some fire tests numerically with FDSv4 [9] and FDSv5 [10] with HRRs from 1.22 MW up to 2.34 MW in the fire atrium located in Spain. The studies on the smoke layer interface highlighted the importance of the make-up air supply or the exhaust flow rate conditions on its behaviour. On one hand, the make-up air supply velocity is reported on the norms [2, 11], to be limited to values below 1 m/s in the flame proximity. However, some studies confirmed that upper values can perturb the flame, increasing the smoke production and reducing the smoke layer interface height, especially for atria heights below 20 m [12–15]. On the other hand, an excessive exhaust flow rate can remove clean air throughout the smoke layer reducing the effectiveness of the smoke exhaust system, effect known as plugholing, which was studied under different smoke exhaust rates and outlet locations by Lougheed et al. [4]. Most of these studies only consider symmetrical make-up air entrainment or constant exhaust flow rates. Therefore, to the best of the authors' knowledge, there is a lack of results on cross-ventilation tests or time-dependent extraction rates. Cross-ventilation can create flow patterns that generate flame disturbances such as swirls or inclinations which may affect the smoke layer interface as well as the fire-induced conditions. And the response of the smoke layer interface when the exhaust flow rate is changed is acutely useful when trying to maintain tenable conditions.

Additionally, how to assess the smoke layer interface is essential due to its importance in the smoke control design. It is usually evaluated in the literature by means of $CO_2$ concentration [16, 17] as well as temperature measurements [18–22], the latter being the most used due to the ease of its measurement. There are many different temperature methods to evaluate the smoke layer interface in the literature, such as the n-percent method proposed by Cooper et al. [18], the upper zone averaging and mass equivalency by Quintere et al. [19], the maximum gradient method by Emmons [20], the Janssen method [21] or the least-square method by He et al. [22]. All these methods, except the least-square method, present a certain grade of empiricism, because of that the least-square method has been used in this paper to compare the smoke layer interface both numerically and experimentally.

With the aim of contributing to the aforementioned subjects, this paper presents results of four new full-scale fire tests with different pool fire sizes, with HRRs of 1.7 MW to 5.3 MW, under different exhaust flow rates and make-up air supply

configurations. Mainly, the smoke temperature in the near (fire plume) and the far field (close to the walls) as well as the smoke layer interface are herein reported. These experimental results could be also used as a benchmark to validate numerical models. In fact, a numerical–experimental comparison using FDSv6 is also presented, validating the numerical model. The paper is structured as follows. Section 2 describes the experimental set-up completely, including the devices used in the fire tests. After that, the experimental tests are detailed in Sect. 3 and the numerical model used is introduced in Sect. 4. Then, in Sect. 5 the results are presented and discussed. And finally, the conclusions are drawn in the last section. Additionally, the study of the heat release rate and the temperature uncertainties on the experiments are described in Appendixes 1 and 2.

## 2. Experimental Set-Up

The experiments have been conducted at the fire atrium located in Murcia, Spain (Figure 1a) [5–8, 23]. This atrium, with dimensions of $19.5 \times 19.5 \times 17.5\,m^3$, has four exhaust fans installed at 1.75 m far from the centre, represented in Figure 1b as "A", "B", "C" and "D". Each fan can work at two different exhaust rates (4.6 $m^3/s$ and 9.2 $m^3/s$). Moreover, vented fire conditions are guaranteed by air entrance through eight identical grilled vents located at the bottom of the atrium, whose dimensions are $4.88 \times 2.5\,m^2$. These openings can be partially or fully opened or closed. The walls and the roof were built with 6-mm-thick galvanized steel, and the ground with concrete, Table 1.

The fire source in the tests herein presented was located at the centre of the atrium and the fuel used was heptane, $C_7H_{10}$. The recipients chosen for the fire tests were circular pool fires normalized with depth of 25 cm. A thin layer of water was also added, with the aim of insulating the fuel from the metal base, to obtain a more stable steady burning regime. The pool fires used and the average
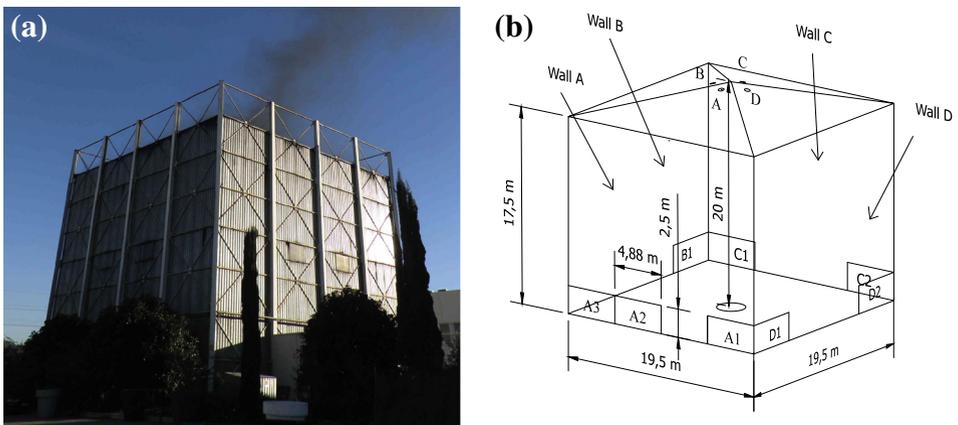
**Figure 1.** (a) Fire atrium. (b) Layout and main dimensions of the atrium.

**Table 1**
**Material Properties of the Facility**

|  | Density (kg/m$^3$) | Thermal conductivity (W/m K) | Specific heat at constant pressure (J/kg K) | Emissivity |
|---|---|---|---|---|
| Galvanized steel | 7800 | 45 | 460 | 0.2 to 0.4 |
| Concrete | 1860 | 0.72 | 780 | 0.9 |

**Table 2**
**Pool Fire Diameters and the Average HRRs Estimated**

| Test | Pool fire diameter (m) | HRR (MW) |
|---|---|---|
| #1 | 0.92 | 1.7 |
| #2 | 1.17 | 2.3 |
| #3 | 1.47 | 3.9 |
| #4 | 1.67 | 5.3 |

HRR estimated are summarized in Table 2. The volume of water was measured before and after each test, observing that this volume remained constant.

The atrium was equipped with a total of 59 thermocouples distributed at different positions to assess the smoke temperature in the fire plume as well as close to the walls. Additionally, three load cells were installed under the pool fire to measure the mass loss rate and determine the HRR of the fire, which will be further described later.

The temperature was measured by means of vertical trees, see Figure 2, at the central section of the atrium, at a distance of 0.3 m from the walls A and C, and close to one of the diagonals of the facility. Moreover, five thermocouples were located at a height of 13.25 m but at different distances from the centre, and another one under fan B. Figure 2a shows a top view of the atrium, in which the different thermocouple trees installed can be observed. Different cross sections of the facility (central section, wall A and wall C) are depicted in Figure 2b–d. Note that the Smoke Layer tree is only included in Figure 2a, which is described in detail later. The three sections considered herein are as follows:

– *Central Section*. Thirteen thermocouples were installed at the centre of the atrium (sensors 1–13), as can be observed in Figure 2b. Some of them were located over the fire to measure the temperature of the fire plume (sensors 1–7), and the one under fan B to measure the maximum smoke layer temperature (sensor 8). Finally, five thermocouples were located at 13.25 m height and every 2 m (except for the sensor 13, Figure 2b) from the centre to characterize the smoke layer radial temperature distribution from the fire source (sensors 9–13).
– *Wall A*. Twelve thermocouples were installed in three thermocouple trees to measure the temperature at 30 cm from the wall A (sensors 14–25) as can be observed in Figure 2c. These measurements are used to study the smoke temperature at the far field and the smoke layer drop.

– *Wall C*. Six thermocouples were installed in two thermocouple trees to measure the temperature at 30 cm from the wall C (sensors 26–31) as can be appreciated in Figure 2d. These measurements also provide information on the smoke layer homogeneity and stability.

– *Smoke Layer Tree*. Twenty-eight thermocouples were installed. From the ground to 5 m height, five thermocouples were installed every meter (sensors 32–36); from 5 m to 15 m height, twenty thermocouples every 0.5 m (sensors 37–56); and from 15 m to 18 m height, three thermocouples every meter (sensors 57–59). This thermocouple tree determines the smoke layer growth as well as the smoke layer response in case of any modification in the ventilation system.

As for the instrumentation, the experimental equipment is as follows:

*Thermocouples*

Bare type K thermocouples with a sensitivity of 41 V/C were installed. The working temperature of these thermocouples ranges from $-200°C$ to $+1350°C$. The wires, with a diameter of 0.5 mm, used to connect the thermocouples with the data loggers, had no unions in order to minimize signal noises. Most of the thermocouple wires were isolated with common fibreglass, which thermally protect the wire up to 400°C. However, the thermocouples located over the fire (sensors 1–5 in Figure 2b) were isolated with high temperature fibreglass, increasing the isolation protection up to 800°C. The uncertainties are described in Appendixes 1 and 2.

*Data Logger*

Three dataTaker DT500 data loggers with 60 independent channels were used to record the thermocouple temperatures. The uncertainties are described in Appendix 1.

*Meteorological Station*

The ambient conditions were taken from a digital barometer Rocktrail, which allowed to measure the temperature, the relative humidity and the pressure outside the facility. The uncertainty of these measurements was 1°C, 5% and 5 mb, respectively.

*Load Cells*

The mass loss rate was measured by means of three Dinacell CF K150 load cells placed under the pool fire. They were insulated with rock wool and covered with aluminium foil in order to minimize the influence of the flame temperature on them. The load cells were connected to a computer by means of a Dinacell ADS 420 digital signal conditioner. Appendix 1 presents the uncertainties related to the mass loss rate, and then for the heat release rate.

## 3. Fire Tests Description

Prior to the experiments presented in this paper some fire tests were carried out in the fire atrium by Gutierrez et al. [5–8], which were used to validate temperatures
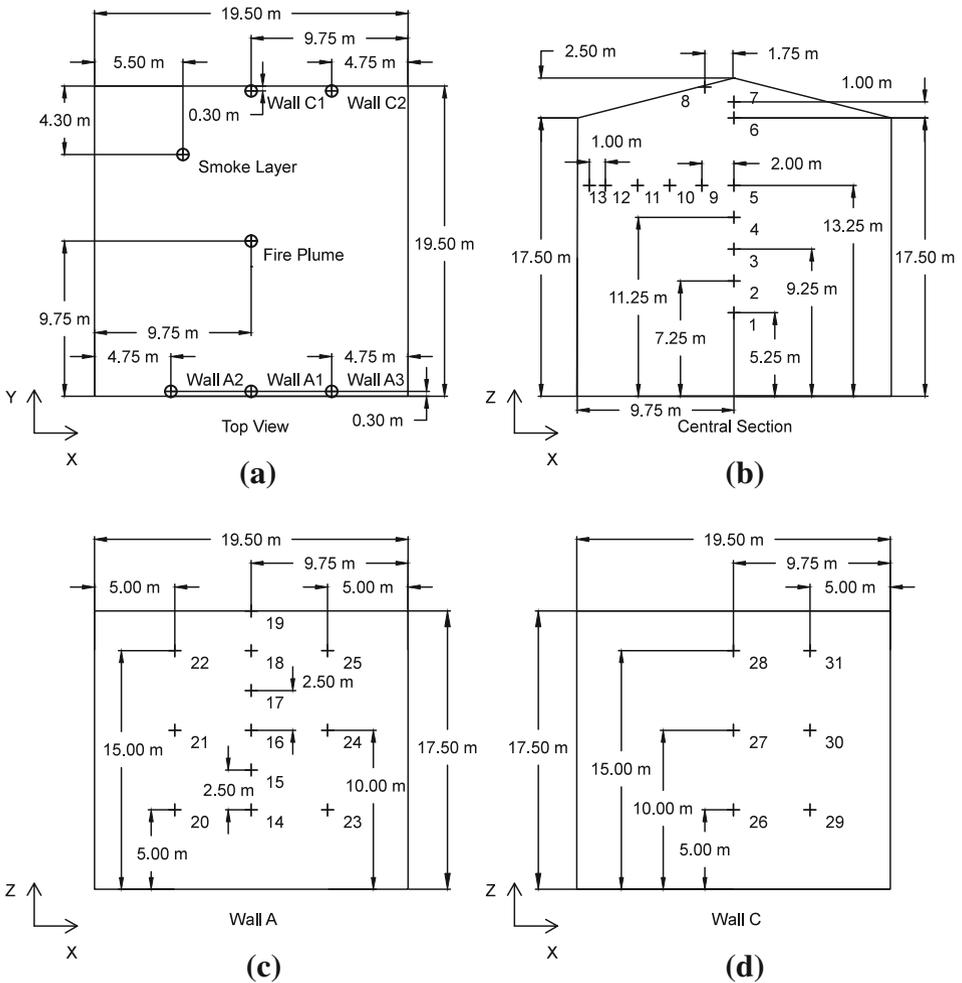
**Figure 2.  Sensors layout on the atrium: (a) thermocouple tree locations, (b) central section, (c) at 30 cm from wall A and (d) at 30 cm from wall C.**

in atrium fires at the fire plume and close to walls under different HRRs using FDSv4 and FDSv5 [10]. Table 3 shows a summary of the tests performance. The set of new fire tests are focused to complement the previous research by means of the study of the smoke layer drop and its response behaviour under time-dependent exhaust flow rates and to assess the make-up air supply configuration and area on the fire-induced conditions.

In this regard, four pan diameters were used in the present work to assess the smoke behaviour and its temporal evolution for a range of heat release rates from 1.7 MW (test #1) to 5.3 MW (test #4). They were located at the centre of the atrium and above three load cells. Heptane was used as fuel, being spilled in the pan.

**Table 3**
**Summary of Experimental Conditions During the Fire Tests Carried Out by Gutierrez et al. [5–8]**

| Fire test | Heptane weight (kg) | Burning time (s) | Open vents | Exhaust flow rate (m³/s) | Amb. temp (°C) | Pressure (Pa) | HRR (MW) |
|---|---|---|---|---|---|---|---|
| Gutierrez et al. [5, 7]—Test #a | 29.5 | 837 | All | 14.32 | 16.7 | 101,800 | 1.5 |
| Gutierrez et al. [6]—Test #b | 35.5 | 1010 | A1, A3, C1, C2 | Note 1 | 13.0 | 101,400 | 1.4 |
| Gutierrez et al. [7]—Test #c | 35.5 | 883 | A1, A3, C1, C2 | 14.32 | 28.9 | 100,800 | 1.6 |
| Gutierrez et al. [7, 8]—Test #d | 35.5 | 1094 | A1, A3, C1, C2 (22%) | 14.32 | 27.5 | 100,700 | 1.3 |
| Gutierrez et al. [6]—Test #e | 51 | 843 | A1, A3, C1, C2 | Note 1 | 18.0 | 101,400 | 2.5 |
| Gutierrez et al. [6]—Test #f | 68 | 1094 | A1, A3, C1, C2 | None | 16.0 | 99,700 | 2.5 |
| Gutierrez et al. [8]—Test #g | 51 | 931 | A1, A3, C1, C2 (22%) | 14.32 | 28.0 | 100,300 | 2.2 |

Note 1: Fans B and D on (7.16 m³/s) and Fans A and C off (natural ventilation throughout the free space on fan holes)

**Table 4**
**Summary of Experimental Conditions During the Fire Tests**

| Fire test | Heptane weight (kg) | Burning time (s) | Open vents | Exhaust flow rate (m³/s) | Amb. temp (°C) | Pressure (Pa) | HRR (MW) |
|---|---|---|---|---|---|---|---|
| Test #1 | 28.8 | 708 | A1, C1 | 18.3 | 20.1 | 101,651 | 1.7 |
| Test #2 | 36.5 | 647 | A1, A3, C1, C2 | 18.3 | 18.0 | 101,617 | 2.3 |
| Test #3 | 54.2 | 836 | A1, A3, C1, C2 | Note 1 | 21.1 | 102,056 | 3.9 |
| Test #4 | 73.0 | 565 | A1, A3, C1, C2 | Note 2 | 16.7 | 102,191 | 5.3 |

Note 1: (0 to 180 s) Natural; (180 to 360 s) 18.3 m³/s; (360 to end) 32.2 m³/s
Note 2: (0 to 270 s) 18.3 m³/s; (270 to end) 27.5 m³/s

Once the fuel was ignited, the fire continued until the fuel was completely burned. Moreover, the openings layout and area as well as the exhaust flow rate were varied to assess the make-up air influence and the mechanical exhaust efficiency. In particular, test #1 considered asymmetrical make-up air venting conditions, whereas test #3 and #4 were conducted under time-dependent ventilation exhaust rates. Table 4 summarizes the experimental conditions of the tests conducted.

The HRR ($\dot{Q}$) has been evaluated by means of the mass loss rate measured by the three load cells as

$$\dot{Q} = \dot{m} \cdot \Delta H_{comb} \cdot \chi_{comb}, \tag{1}$$

where $\dot{m}$ is the mass loss rate, $\Delta H_{comb}$ the heat of combustion which is 44.647 MJ/kg for heptane, and $\chi_{comb}$ the combustion efficiency which is 0.92 [24].

Figure 3 shows the HRR curves with the uncertainty bounds for the different tests. Different behaviours can be observed. In test #1, which pan diameter is 0.92 m (Figure 3a), the average HRR is 1.7 MW. It is possible to appreciate different peaks with values that reach up to 7.3 MW, which are not expected for this pan
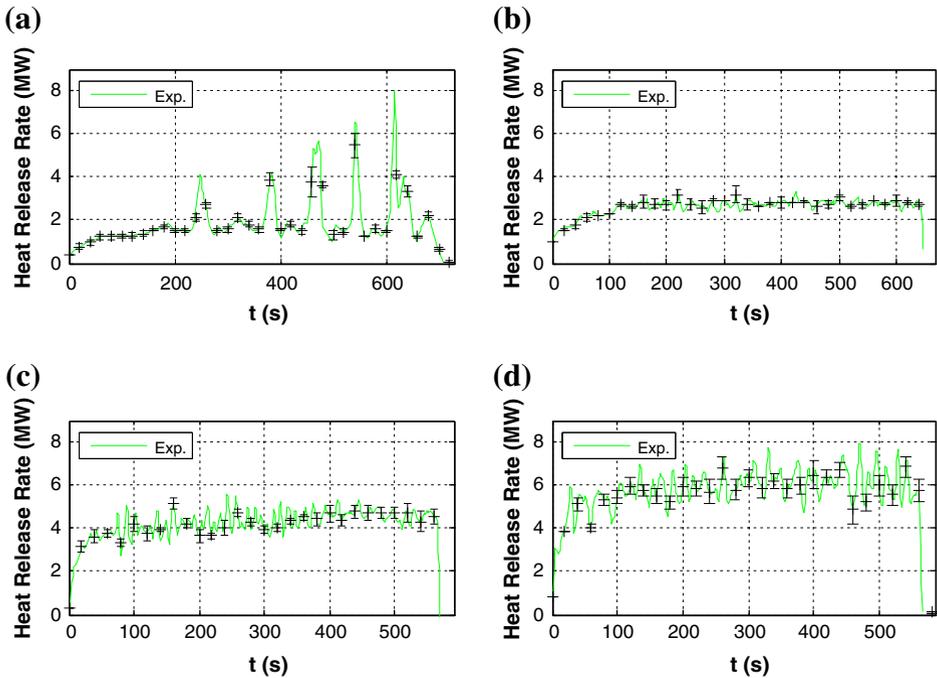
**(a)**



**(b)**



**(c)**



**(d)**



**Figure 3.   Heat release rate curves with uncertainty bounds. (a) test #1, (b) test #2, (c) test #3 and (d) test #4.**

size whose value should be around 1.5 MW [6]. Those peaks are caused by the make-up air flow induced by the asymmetrical opening distribution, being capable to produce flame swirls which are translated into high heat release rates. In contrast, test #2, which pan diameter is 1.17 m and the average HRR is 2.3 MW (Figure 3b), shows small oscillations. The third pan used, test #3, with a diameter of 1.47 m corresponds to an average HRR of 3.9 MW (Figure 3c). Finally, the largest pan used in test #4 with a diameter of 1.67 m presents an average HRR of 5.3 MW (Figure 3d).

# 4. Numerical Set-Up

As it has been previously commented, Fire Dynamic Simulator (FDSv6) [1] has been used to carry out the numerical simulations. The models used to account for combustion, turbulence and radiation were the Eddy dissipation concept (EDC) model with a thermal extinction model, Deardorff model ($C_v = 0.1$) and radiation transport equation with 100 radiation angles, respectively [1]. As boundary conditions, the walls and the pyramidal roof were modelled with 6 mm thermally thick galvanized steel (Table 1). The ground floor was simulated as a thermally thick layer of concrete, Table 1. The fans were modelled as flow rate curves corresponding to the temporal exhaust flow rates, and the make-up air inlets at the bottom

of the atrium as open vents. The outer atmospheric conditions, shown in Table 4, are imposed considering quiescent atmosphere.

The pool fire was modelled setting the estimated HRR curves as an input for each test (Figure 3). The radiation fraction for the heptane was 0.35 [6].

Finally, the grid size has to be small enough to properly model the turbulence effects. For the LES method, a spatial resolution of $1/4 < R < 1/16$ is recommended [25]. This spatial resolution is defined as $R = \Delta/D^*$, where $\Delta$ is the element size and $D^*$ the characteristic diameter of the plume, obtained from the Froude number [24], calculated as

$$D^* = \left( \frac{\dot{Q}}{\rho_\infty c_{p,\infty} T_\infty \sqrt{g}} \right), \tag{2}$$

where $\dot{Q}$ is the HRR (kW), $\rho_\infty$ is the air density (kg/m$^3$), $c_{p,\infty}$ is the air specific heat at constant pressure (J/kg K), $T_\infty$ is the air temperature (K) and g is the gravity acceleration modulus (9.81 m/s$^2$) [26].

Figure 4 presents a sensitivity analysis of the element size (20 cm, 13 cm and 10 cm) for test #1, which shows the results obtained at h = 15 m, h = 10 m and h = 5 m near the wall A. It can be observed that the two finer grids, i.e. grids of 10 cm and 13 cm, present the same results, whereas the coarsest grid predicts slightly different results, but close to those from the two finer grids. In the present study, the element size chosen for this paper was 13 cm, the minimum resolution being 1/9 for test #1 and the maximum resolution 1/14 for test #4, within the aforementioned recommendation, in order to optimize the computational cost of the computations, considering that it takes 1150 s to simulate 1 s of fire test in the case of the finest grid, whereas it takes 370 s in the case of the 13 cm grid cell.

## 5. Results

As it has been previously commented, the main experimental and numerical results are presented and discussed in this section. Four different pool fires with diameters of 0.92 m, 1.17 m, 1.47 m and 1.67 m have been assessed. These tests
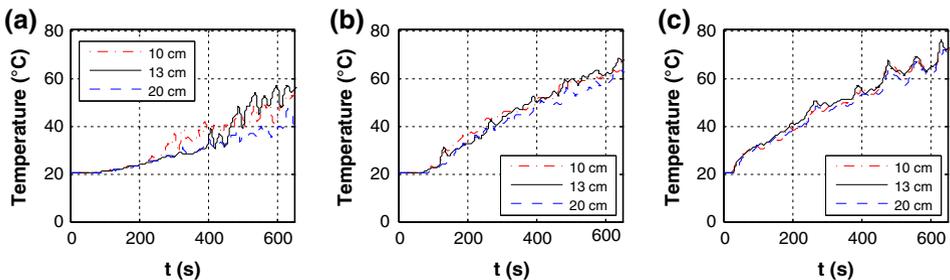


**Figure 4. Test #1. Temperatures at 30 cm from Wall A at (a) h = 5 m, (b) h = 10 m and (c) h = 15 m.**

presented are carried out under different exhaust flow rates as well as different make-up air supply configurations. To this aim, thermocouples in the near field as well as in the far field have been used to characterize the main features of the fire-induced inner conditions. Furthermore, the dynamic behaviour of the smoke layer interface has also been assessed by varying the exhaust flow rate during some experiments. The above measurements have been compared with the corresponding results from simulations by means of absolute and relative differences, the latter being calculated with respect to the experimental results. Additionally, two previous fire tests carried out by Gutierrez et al. [6, 7] in the fire atrium have been also simulated with FDSv6 in order to analyse the robustness of the model herein presented.

The smoke layer height has been also studied by means of the "Smoke Layer" thermocouple tree (Figure 2a). The least-square method [13, 27] as well as the n-percent (N = 30%) method [14, 26] have been assessed by means of absolute and relative discrepancies, the latter being calculated with respect to the total atrium height (20 m). These two methods have been used to assess their accuracy in representing the smoke layer height. On one hand, the n-percent method has been one of the most extended methods to determine the free smoke height [6, 28], due to the ease of calculation. On the other hand, the least-square method is neither dependent on any parameter nor empirical correlations [22]. This method, applied to the smoke temperature, establishes the smoke layer interface where the deviation ($\sigma_d$) of the temperature at the smoke layer interface is minimum. This deviation is defined as follows:

$$\sigma_d(H) = \frac{1}{H}\int_0^H [T(z) - T_l]^2 dz + \frac{1}{H_t - H}\int_H^{H_t} [T(z) - T_l]^2 dz \tag{3}$$

$$T_l = \frac{H_i}{\int_0^H 1/T(z)dz}, \tag{4}$$

where $H$ is the height of the smoke layer interface, $H_t$ the total height of the atrium and $T(z)$ the temperature at a height $z$. Therefore, for a given vertical temperature profile, the least-square smoke interface $H_i$ is that which minimizes the deviation:

$$\sigma^2(H_i) = min[\sigma^2(H)]. \tag{5}$$

These methods require to be updated every time step to obtain the smoke layer descent. Additionally, ghost thermocouples have been introduced every 10 cm by means of interpolation between the thermocouples originally installed in order to acquire more accuracy in the smoke layer interface position. The smoke layer has also been numerically evaluated by means of least-square method applied on the same thermocouple locations as in the experiments.

## 5.1. *Previous Tests Validation with FDSv6*

Test #c and test #e were carried out by Gutierrez et al. [6, 7] using pans of diameters 0.92 m and 1.17 m, respectively, with the average estimated HRRs of 1.6 MW and 2.5 MW, respectively. Both tests used a symmetrical inlet vent distribution (A1, A3, C1 and C2 opened). Test #c was fully mechanically ventilated (14.32 $m^3$/s), whereas a mix of natural and mechanical ventilation were chosen in Test #e (fans B and D on, 7.16 $m^3$/s, and A and C off).

Figure 5a–f show the temperature profiles at 5.25 m height over the fire (a, d), under fan B (b, e), and at 5 m height at 30 cm from wall A (c and f) of Test #c and Test #e, respectively. On the fire plume (Figure 5a, d), higher differences can be observed during the beginning of the fire tests. Additionally, it can be observed that the temperature profiles take some time to reach higher temperatures, whereas the simulations reach these values almost instantly once the fire had begun. This effect may be associated to the thermal inertia of the thermocouples used in this experiment, which were sheathed probes of 3 mm diameter. In the case of the new experimental data presented in next subsections of this paper, 0.5 mm bare thermocouples were used, with a significantly lower thermal inertia. This phenomenon is also observed under fan B (Figure 5b, e), in which higher temperatures were predicted during the first 400 s of simulation. The maximum discrepancy in the last 100 s of simulation is 3°C (3%) and 18°C (18%) for Test #c and #e, respectively. Finally, the temperature at 5 m height close to wall A is
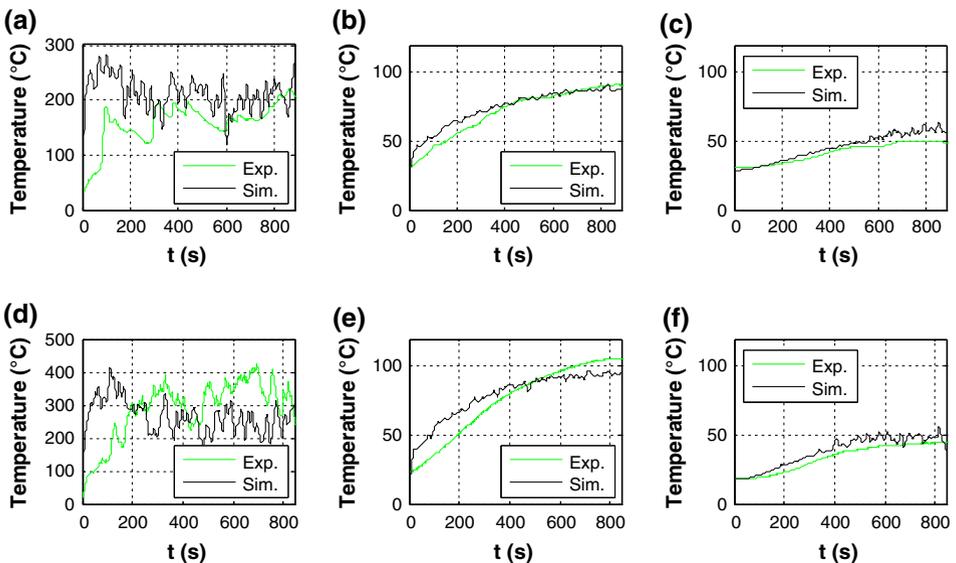


**Figure 5.   Temperatures in the fire plume at (a, d) h = 5.25 m; under fan B (b, e); and at 30 cm from Wall A at 5 m (c, f). Test #e is represented in (a–c), and Test #d in (d, e).**
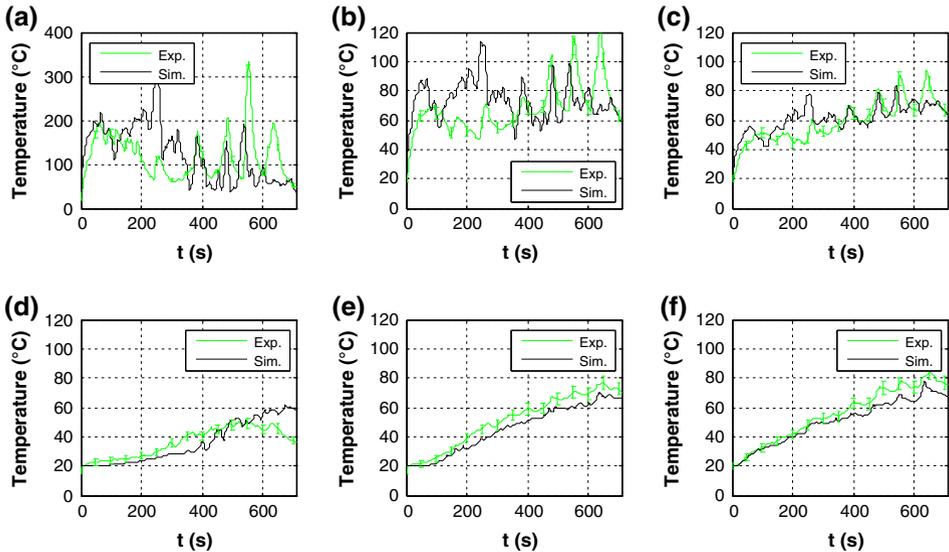
**Figure 6. Test #1. Temperatures and experimental uncertainty bounds. Fire plume at (a) h = 5.25 m (sensor 2), (b) h = 7.25 m (sensor 4), and (c) h = 13.25 m (sensor 6). At 30 cm from Wall A at (d) h = 5 m (sensor 14), (e) h = 10 m (sensor 16) and (f) h = 15 m (sensor 18).**

quite well predicted, the average discrepancy during the last 200 s, once the steady state is reached being 4°C (10%) and 7°C (15%) for Test #c and #e, respectively.

## 5.2. Test #1

Test #1 was carried out with a pan of diameter equal to 0.92 m and an estimated average HRR of 1.67 MW. Cross-ventilation was imposed with vents A1 and C1 opened (Figure 1). A constant exhaust flow rate of 18.3 m$^3$/s was established.

Figure 6a–c show the near-field temperature, specifically the fire plume temperatures at h = 5.25 m, 7.25 m and 13.25 m (sensors 2, 4 and 6). The temperature at this region is very high due to the proximity to the flame and the combustion products are not diluted with air, above all at 5.25 m (Figure 6a). The temperature decreases as the height increases due to the make-up air entrainment to the fire plume (Figure 6b, c). These measurements are highly affected by flame local effects, e.g. flame inclinations. In addition, three experimental temperature peaks can be clearly appreciated after 400 s, which can be explained as a consequence of the flame swirls provoked by the cross make-up air supply distribution. This open vents distribution causes a flow pattern which creates flame swirls, as can be observed in Figure 7b, which increases the mass loss rate, i.e. the HRR, as well as the flame height. These flame swirls, and the consequent temperature increments, affect the fire-induced conditions not only in the near field, but also in the far field (Figure 6d–f). The comparison with the simulation shows the same gener-
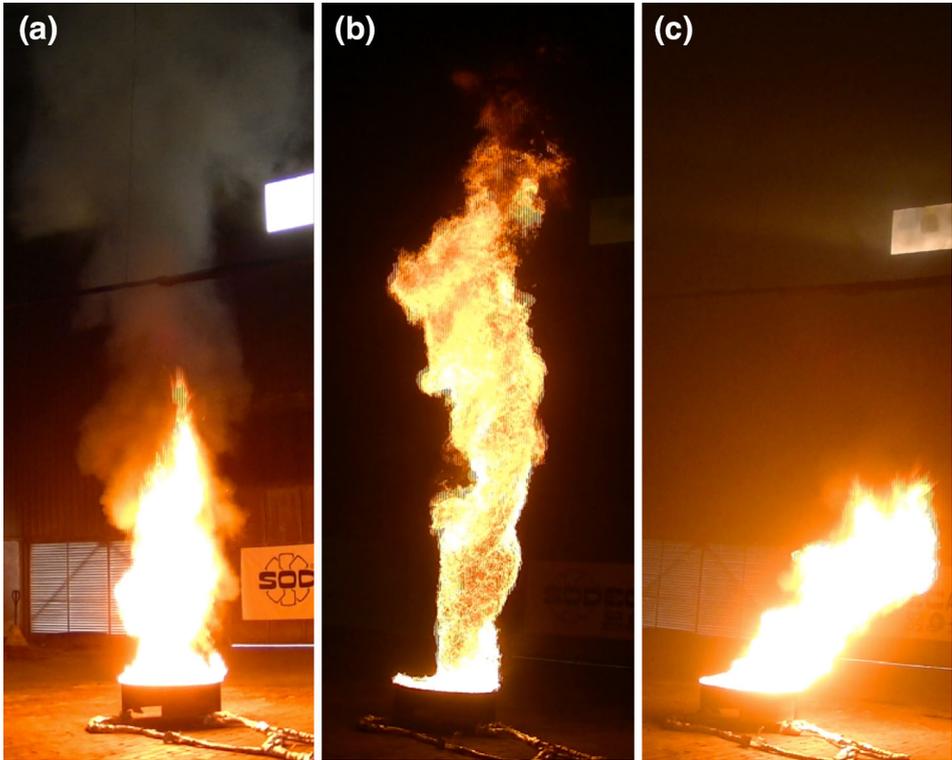
**Figure 7.   Pictures of Test #1 after (a) 64 s, (b) 623 s and (c) 662 s.**

al trend with a fairly good agreement, considering the above-mentioned phenomena affecting the flame. However, this agreement is better at greater heights, i.e. 7.25 m and 13.25 m, due to the lower influence of the flame on these regions. Moreover, the major temperature differences can be found at the early stages t < 300 s at h = 5.25 m and 7.25 m. A numerical swirl after 200 s is predicted due to the peak in the mass loss rate introduced (Figure 6a). However, its inclination has not been properly simulated as can be appreciated by the discrepancies observed.

With respect to the far field, Figure 6d–f present the temperature measurements at three sensors close to wall A (sensors 14, 16 and 18). The temperature at this region is lower and starts to rise later as a consequence of the travelling time of the smoke from the fire plume to the smoke layer and its subsequent growth. In general, the same trends are noticed in the experiments and the simulations. Quite good agreement is also obtained in the other regions with average discrepancies of 5°C (8%), 6°C (11%) and 6°C (17%) at 15 m, 10 m and 5 m height, respectively. Furthermore, the largest discrepancies are observed at 5 m hheight, where experimentally a sudden temperature drop occurs at the final stages at approximately 635 s, whereas in the simulation the temperature continues to increase. This can
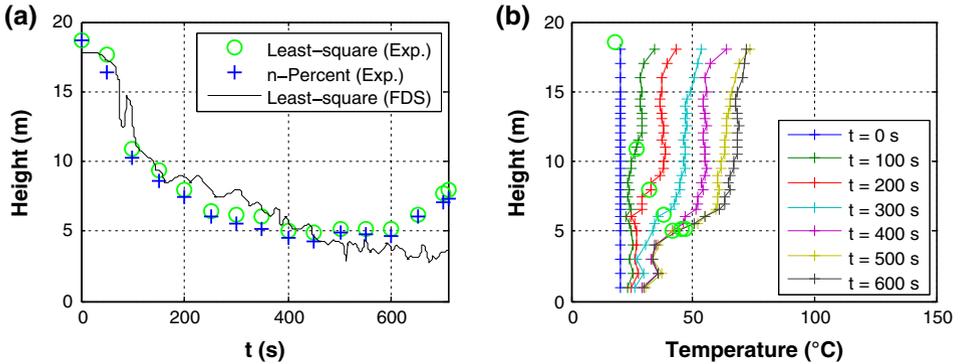
**Figure 8.  Test #1. (a) Smoke layer drop. (b) Experimental smoke layer temperature profiles every 100 s.**

be explained because of a flame inclination during the test which can be observed in Figure 7c.

Finally, Figure 8 shows the smoke layer drop and the experimental vertical temperature profiles every 100 s. Experimentally, the n-percent method predicts a slightly more conservative smoke layer height than the least-square method, detecting the initial smoke layer drop earlier, as can be observed at 50 s. From then on, a maximum difference of 1.6 m (8%) is obtained, the average discrepancy being 0.6 m (3%). This is a very important issue because such a difference can imply the death of the occupants or it can lead to a non-efficient or too expensive smoke exhaust system. When compared to the simulation, the smoke layer interface shows the same trend. Numerically, the difference with respect to the experimental measurements is more perceptible, above all, during the smoke layer drop (200 s and 400 s), with differences of 2.4 m (12%). It can be noticed that until 200 s the values (experimental and numerical) present a similar behaviour with an average difference lower than 1 m (5%). Then, the numerical smoke layer height is larger up to 400 s, when the numerical prediction becomes lower than the experimental one, reaching the steady state at 450 s, with discrepancies of 1 m (5%). These discrepancies could be caused by the aforementioned flame swirls which are very difficult to be modelled accurately. Moreover, it is worth highlighting that after 620 s the experimental results show an increase in the smoke layer interface, which can be associated to a reduction in the smoke production due to the flame inclination described previously.

### 5.3. Test #2

Test #2 was conducted with a pan of 1.17 m, the average estimated HRR being 2.4 MW, with a symmetric inlet vents distribution (A1, A3, C1 and C2 opened) and with a constant exhaust flow rate (18.3 m$^3$/s).

Figure 9a–c present the fire plume temperature evolution at 5.25 m, 9.25 m and 13.25 m height (sensors 2, 4 and 6). It can be appreciated in Figure 9a, b that the
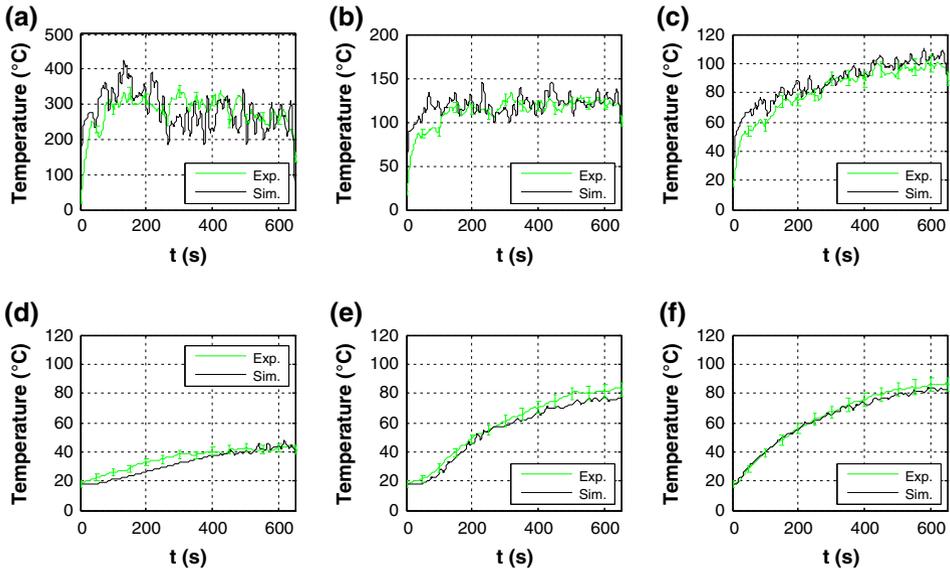
**Figure 9.** **Test #2. Temperatures and experimental uncertainty bounds. Fire plume at (a) h = 5.25 m (sensor 2), (b) h = 7.25 m (sensor 4), and (c) h = 13.25 m (sensor 6). At 30 cm from Wall A at (d) h = 5 m (sensor 14), (e) h = 10 m (sensor 16) and (f) h = 15 m (sensor 18).**

flame reaches a steady state after 300 s at 5.25 m and 9.25 m height, the average differences between the model and the experimental results being 16°C (5%) and 15°C (14%). Also, the predicted temperature at 13.25 m height (Figure 9c) agrees well with the experimental values. The steady state is reached in the last 100 s, obtaining a difference of 14°C (12%). Predicted temperatures are in general slightly higher than the real measurements, notwithstanding the overall agreements are good.

As for the temperature recorded close to wall A, Figure 9d, e show a good agreement with the experimental results. At 10 m and 15 m height (Figure 9e, f), it can be seen the steady state is not reached. Thus, a mean value of the temperature cannot be considered to compare with the numerical model, being more adequate the use of the relative differences of the temperature at each time step. The largest relative discrepancy reached is 12.5°C (30%) at 5 m height, at 470 s. The differences in the rest of the thermocouples are lower than 7%.

Concerning the smoke layer drop, a common behaviour can be appreciated in Figure 10a, in which three main parts can be clearly differentiated: the smoke filling, the smoke layer drop and the steady state. Experimentally, the n-percent method is more conservative than the least-square method, the difference at the steady state being lower than 1 m. Numerically, the simulation predicts very well the smoke layer interface, although the smoke drops slightly slower, reaching the steady state after 400 s (h = 5.2 m) whereas numerically at 300 s approximately
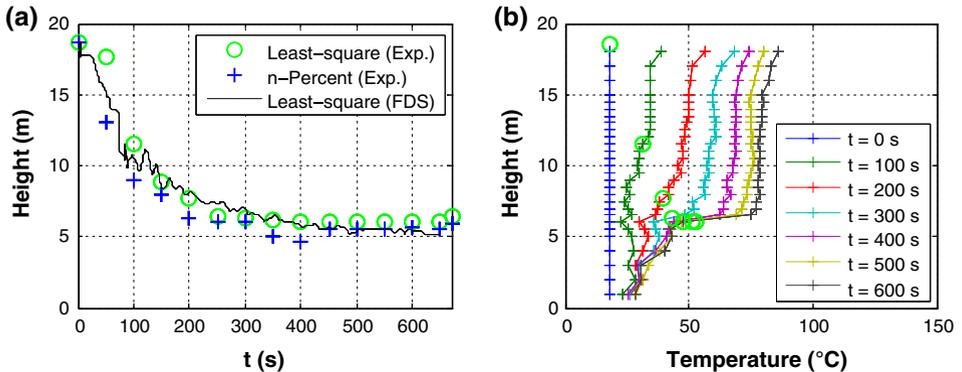
**Figure 10. Test #2. (a) Smoke layer drop. (b) Experimental smoke layer temperature profiles every 100 s.**

(h = 6.1 m). Experimentally, it can be also appreciated in the smoke layer temperature profile (Figure 10b), in which the smoke layer interface is clearly identified after 300 s.

### 5.4. Test #3

Test #3 was carried out with a pan of diameter 1.47 m, with an average HRR of 3.9 MW. The make-up inlet vents topology was the same as in test #2, i.e. symmetrical configuration with A1, A3, C1 and C2 opened. As for the exhaust rate, non-constant exhaust flow rate was considered. In particular, all the fans were off at the beginning, i.e. natural ventilation until t = 180 s, when all of them were switched on with a total flow rate of 18.3 m$^3$/s. At t = 360 s, the exhaust rate was increased up to 32.2 m$^3$/s. This test and test #4 were conducted to assess the effect of a time-dependent extraction rate on the smoke layer growth, the possible transient effects due to the exhaust regime variations and the ability of FDS to properly predict the induced conditions.

If the near field is considered, Figure 11a–c show the temperatures at three different heights of the fire plume, sensors 2, 4 and 6. In the experiments, the measurements are fairly stable, which indicate that the flame remained vertical most of the time, presenting small variations that can explain the subsequent discrepancies with the predictions. The temperatures are also higher than in the previous tests as the HRR is significantly larger. Furthermore, at h = 13.25 m three smoke temperature increment trends can be distinguished, corresponding with the above-mentioned exhaust conditions. The comparison with the simulation shows a quite good agreement, the temperature being slightly over-predicted, with the average discrepancies of 44°C (10%), 25°C (17%), and 21°C (19%) at 5.25 m, 7.25 m and 13.25 m height, respectively, evaluated from t = 200 s (steady combustion regime).

With respect to the temperature of the smoke close to the wall A (Figure 11d–f), the measurements also show three different temporal evolutions. Moreover, the
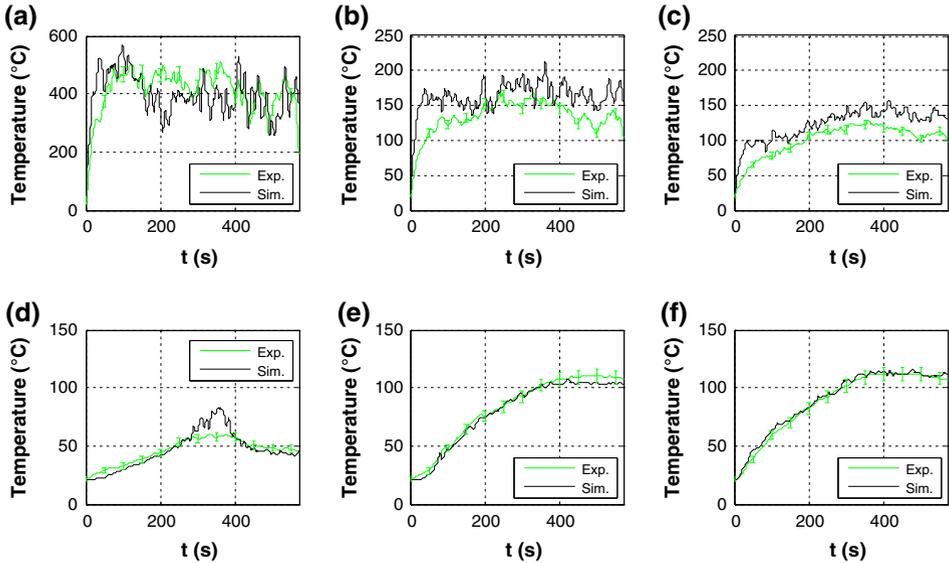
**Figure 11. Test #3. Temperatures and experimental uncertainty bounds. Fire plume at (a) h = 5.25 m (sensor 2), (b) h = 7.25 m (sensor 4), and (c) h = 13.25 m (sensor 6). At 30 cm from Wall A at (d) h = 5 m (sensor 14), (e) h = 10 m (sensor 16) and (f) h = 15 m (sensor 18).**

agreement with the numerical predictions is remarkably good. As it has been commented, at 5 m height (Figure 11d), both experimentally and numerically, the smoke exhaust flow rate increment can be clearly observed after 360 s causing a temperature drop. At this location, there are certain discrepancies at t $\approx$ 300 s, which could be caused by a small difference in the smoke travelling velocity or a predicted larger smoke layer interface mixing due to the exhaust flow rate change. However, these differences are magnified by the location of the interface at this height approximately, as observed in Figure 12. Consequently, the subsequent numerical smoke temperature descent at t > 360 s is larger, although the final temperature is well predicted. At the remaining heights, that is 10 m and 15 m height (Figure 11e, f), the average differences are of 3°C (5%) and 2°C (3%), respectively.

Regarding the smoke layer (Figure 12a), a fast growth can be appreciated at the early stages, due to the low exhaust rate (natural ventilation), the large HRR of the fire and the total height of the facility. This growth decreases with time as the smoke descends and due to the exhaust flow rate variation. As it has been commented before, these different exhaust rates can be clearly identified, above all the change from 18.3 m³/s to 32.2 m³/s, at t = 360 s, which induces a quite noticeable increment in the clear height, from 5.6 m to 7.5 m, which can also be appreciated in the experimental smoke temperature profiles (Figure 12b). Again, certain discrepancies between the two methods used to experimentally determine the

smoke layer height have been found, with the n-percent method presenting a lower height, with a maximum difference of 1.2 m (6%). Although this extreme value is significant, the average discrepancy is 0.4 m (2%). Moreover, the predicted smoke layer height shows a remarkably good agreement with the experimental data, even considering the time-dependent exhaust flow rate. From t = 100 s to 180 s, when the fans are off, the predicted smoke layer drop does not present any clear difference with the experiments, this being always lower than 1 m (5%). Then, when the fans are switched on, with a 18.3 m$^3$/s flow rate, there is still a good agreement. Finally, when the exhaust flow rate was increased up to 32.1 m$^3$/s and the smoke layer begins to ascend, the differences for the last 50 s are lower than 0.3 m (3%).

## 5.5. Test #4

Test #4 was carried out using a pan of diameter 1.67 m, with an average estimated HRR of 5.3 MW. Again, a symmetrical make-up air supply distribution (A1, A3, C1 and C2 opened) and a non-constant exhaust flow rate were considered. In this test, the four fans were switched on from the test beginning with an exhaust flow rate of 18.3 m$^3$/s, and after 270 s the exhaust rate was increased up to 27.5 m$^3$/s.

Figure 13a–c show the smoke temperature at different heights of the fire plume. At 5.25 m and 7.25 m height (Figure 13a, b), large temperature oscillations can be noticed from t > 200 s, which indicate that the flame was not completely vertical. Despite these local effects, the comparison with the simulation shows that after 200 s, i.e. once a steady combustion regime is reached, the average discrepancies are 63°C (13%) and 39°C (23%), respectively, the temperature being slightly over-predicted. At 13.25 m height (Figure 13c), the temperature is well predicted, with a maximum discrepancy at t = 450 s of 47°C (32%), and an average difference of 25°C (17%).
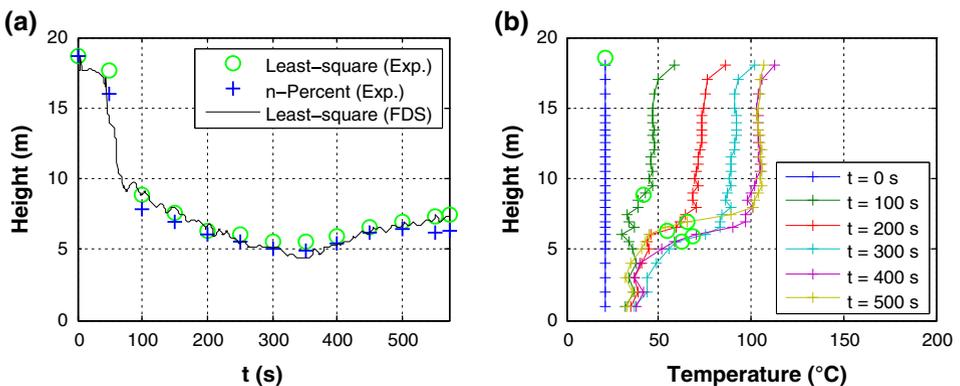


**Figure 12.   Test #3. (a) Smoke layer drop. (b) Experimental smoke layer temperature profiles every 100 s.**
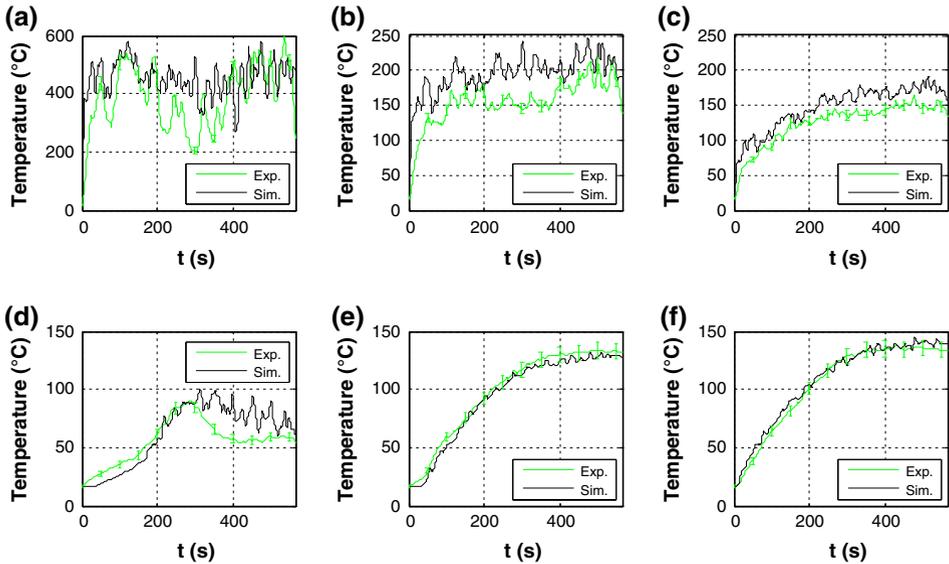
**Figure 13.  Test #4. Temperatures and experimental uncertainty bounds. Fire plume at (a) h = 5.25 m (sensor 2), (b) h = 7.25 m (sensor 4) and (c) h = 13.25 m (sensor 6). At 30 cm from Wall A at (d) h = 5 m (sensor 14), (e) h = 10 m (sensor 16) and (f) h = 15 m (sensor 18).**

As for the thermocouples close to wall A (Figure 13d–f), a continuous temperature increment is observed until $t \approx 450$s, when the fire-induced conditions reach a steady state. Again, the exhaust rate change is noticeable, above all at h = 5 m, where a significant temperature drop occurs. In general terms, the predicted values agree well with the experimental ones at the higher locations. Furthermore, at the final stages, average discrepancies of 1.5°C (10%), 15°C (14%) and 7.5°C (6%) are observed at h = 5 m, 10 m and 15 m, respectively. The major differences are found at 5 m height, after the exhaust rate was increased. Experimentally, a fast temperature drop occurs, as previously commented, whereas numerically the temperature reduction is slower. The predicted final state agrees well in terms of temperature, which can indicate that FDS predicts a larger mixing at the smoke layer interface.

If the smoke layer and the experimental smoke temperature profile are considered (Figure 14), the effect of the time-dependent exhaust rate can be clearly noticed in the experiments, where a smoke layer height increment occurs after $t$ = 270 s. The two methods assessed determine similar heights. However, when compared with the simulation, there is good agreement up to $t$ = 270 s. i.e. before the exhaust rate is modified. From then on, FDS predicts a lower smoke height, in accordance with the above-mentioned possibility of a predicted larger mixing at the smoke layer interface. As a consequence, a final clear height of 5.4 m is achieved, the experimental one being equal to 6.8 m, i.e. 7% difference.
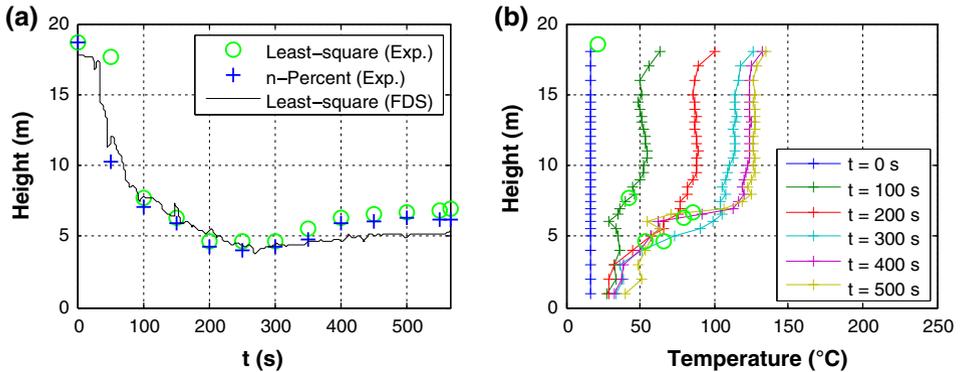
**Figure 14.   Test #4. (a) Smoke layer drop. (b) Experimental smoke layer temperature profiles every 100 s.**
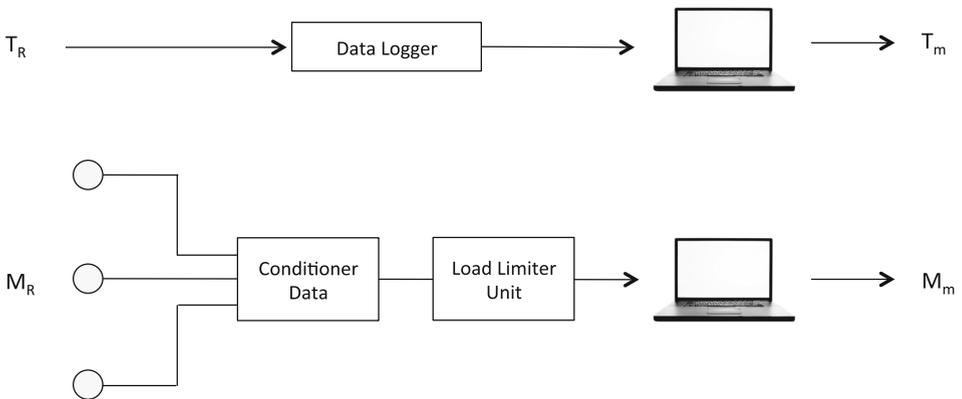


**Figure 15.   Propagation uncertainty scheme.**

## 6. Conclusions

This paper presents results from four novel fire tests of 1.7 MW, 2.3 MW, 3.9 MW and 5.3 MW under different exhaust conditions (steady and transient extraction rates) and make-up air configurations (symmetric and asymmetric) to assess their effect on the fire induced conditions. This has been studied by means of temperature measurements in the near (fire plume) and far field (close to wall). Additionally, the smoke layer interface has been presented and compared.

In this regard, a good agreement has been found in the four fire tests between the numerical data and the experimental measurements in the near field, and also in the far field. In the near field, the numerical temperature is slightly over-predicted, with average discrepancies lower than 32% in all the tests, obtaining the larger differences for higher HRRs. In the far field, the temperatures predictions

are fairly accurate inside the smoke layer (10 m and 15 m), whereas larger discrepancies were observed at the smoke layer interface, i.e. 5 m high. The discrepancies at 10 m and 15 m high are lower than 11%, whereas at 5 m discrepancies up to 30% can be found, which is within the uncertainty associated to FDS [25].

Both kinds of exhaust flow rates herein considered, i.e. steady (test #1 and #2) and transient extraction rates (test #3 and #4), are well predicted. The smoke layer interface with a steady exhaust rate is slightly under-predicted, the discrepancy found being lower than 1 m (5%) once the steady state is reached. And under transient exhaust conditions, the smoke layer growth is predicted accurately, observing a larger mixing prediction at the interface, which affects the predicted temperature at 5 m high, although with a small effect on the smoke layer height.

Finally, it is worthy highlighting that FDSv6 is able to predict well the fire induced conditions in all cases when the measured HRR of the fire is an input. This confirms that the HRR plays an essential role in fire simulations and must be accurately modelled or set as input.

## Acknowledgments

## Appendix 1: Propagation Uncertainties

In real measurements, the signals identified by devices are transmitted, in most of the cases, by wires going through signal conditioners before being translated into measurements. During this signal path, different devices are crossed. In the tests described herein, measurements of temperature and mass loss rate were taken. On one hand, the temperature was measured with thermocouples type K connected directly by wires to a data logger which was connected to a computer. And on the other hand, the mass loss rate was measured with three load cells located under the pan. These were connected with an unified signal box and a load limiter unit which was directly plugged in a computer. Figure 15 shows both data acquisition schemes.

On the one hand, thermocouples uncertainties are as follows:

– Thermocouple type K: Class 2, according to IEC 584, $\Delta T_{TC} = \pm 2.2$ °C and $\Delta_S^{Te} = \pm 0.75\%$ for T > 333°C, being null for temperatures lower.
– Data logger, *dataTaker DT500*, $\Delta T_{DL} = \pm 0.1$°C and $\Delta_{DT}^T = \pm 0.1\%$.

Therefore, the total uncertainty when measuring the temperature is

$$u_{T_m}^2 = u_{\Delta_S^{T_e}}^2 + u_{\Delta_{DT}^T}^2 + u_{\Delta T_{TC}}^2 + u_{\Delta T_{DL}}^2 + u_{\Delta T_{rad}}^2 . \tag{6}$$

On the other hand, the uncertainties related to the mass loss rate measurement are as follows:

– Load cell, according to the manufacturer, *Dinacell*, $\Delta_{LC} < 0.027\%$ of rated output.
– Conditioner data, according to the manufacturer, *Dinacell*, $\Delta_{BA} \sim 0\%$
– Load limiter unit, according to the manufacturer, *Dinacell*, $\Delta_{LL} = \pm 0.3\%$.

Thus, according to Eq. (1), the total uncertainty for the HRR is evaluated as

$$u_{HRR}^2 = \left(\frac{\partial \dot{Q}}{\partial \Delta m}\right)^2 \cdot u_{\Delta m}^2 + \left(\frac{\partial \dot{Q}}{\partial \Delta t}\right)^2 \cdot u_{\Delta t}^2 + \left(\frac{\partial \dot{Q}}{\partial \Delta H_{comb}}\right)^2 \cdot u_{\Delta H_{comb}}^2 . \tag{7}$$

The values obtained from the previous expressions have been represented in Figures 3, 6, 9, 11 and 13.

## Appendix 2: Heat Transfer Mechanisms Thermocouple Corrections

The smoke temperature is measured by thermocouples, but some corrections are necessary due to heat transfer mechanisms (mainly convection and radiation). Moreover, considering the thermal inertia of the thermocouples, the variation of the temperature measured is many times faster than the thermal lag times, the latter being then neglected. Based on that, it is possible to assume steady-state conditions, and to split the net heat flux into radiative and convective:

$$\dot{q}_{net}'' = \dot{q}_{rad}'' + \dot{q}_{conv}'' = 0 \tag{8}$$

$$\dot{q}_{rad}'' = \epsilon_{TC}\sigma\left(T_s^4 - T_{TC}^4\right) \tag{9}$$

$$\dot{q}_{conv}'' = h_{TC}\left(T_{gas} - T_{TC}\right), \tag{10}$$

where $T_s$ is the effective surroundings temperature, $\sigma$ is the Stefan–Boltzmann constant of $5.670373 \times 10^{-8}$ W/m$^2$ K$^4$ and $\epsilon$ is the emissivity whose value is between 0.8 and 0.9 [29, 30]. Also, $h_{TC}$ is the convective heat transfer coefficient obtained from Nusselt number definition as $h_{TC} = \frac{k \cdot Nu}{d_{TC}}$, the thermal conductivity of the fluid,

$k$, and $d_{TC}$ which is the diameter of the thermocouple, considered three times the wire diameter (0.5 mm) [29].

The thermal conductivity is evaluated as $k = \mu c_p / Pr$ where the Prandtl number, $Pr$, and the specific heat, $c_p$, are considered constant with values of 0.5 kJ/kg K and 1 kJ/kg K, respectively [31].

The viscosity, $\mu$, is assessed by the Sutherland's formula as a function of temperature, $\mu = C_1 T^{3/2} / (T + C_2)$. Air is considered as the dominant fluid on the smoke, and then the coefficients values are $C_1 = 1.458 \times 10^{-6}$ kg/ms $K^{1/2}$ and $C_2 = 110.4$ K [32].

The Nusselt number can be evaluated for a sphere using the correlation of William–Kramer, $Nu = Re^{0.6}$, defining the Reynolds number as $Re = \rho_{gas} U d_{TC} / \mu$ in which $U$ is the external fire-induced low velocity (0 m/s to 2 m/s). The density of the gas is evaluated from the ideal gas law correlation $\rho_{gas} = \rho_{amb}(T_{amb}/T_{gas})$.

Therefore, re-writing the Eqs. (8)–(10), the gas temperature can be shown as

$$T_{gas} = T_{TC} + \frac{\epsilon_{TC}\sigma}{h_{TC}} \left( T_{TC}^4 - T_s^4 \right) \tag{11}$$

The effective surrounding temperature $T_s$ has to be calculated for each thermocouple at each time step under the influence of the rest of thermocouples as

$$T_s = \sqrt[4]{W_1 T_{gas,TC1}^4 + W_2 T_{gas,TC2}^4 + W_3 T_{gas,TC3}^4 + \cdots + W_n T_{gas,TCn}^4}, \tag{12}$$

where $W_i$ is the weighting factor of every thermocouple. This factor is calculated by the normalized products of the transmissivity between thermocouples and the emissivity of the volume of gas around thermocouple $i$ [30]:

$$W_{i=1}^n = \frac{e^{L_i\kappa}(1 - e^{\Delta L_i\kappa})}{\sum_{i=1}^n e^{L_i\kappa}(1 - e^{\Delta L_i\kappa})} \tag{13}$$

$L_i$ is the relative effective distance between thermocouples, and $\kappa$, which is the optical medium property, is considered locally constant (0.8 to 1). And $\Delta L_i$ is considered the length related to emissivity. This depends on the distance and the path of the gas from the origin, being then for the thermocouples arranged in the same direction (same thermocouple tree) as $L_2$ at $i = 1$, $(L_{n+1} - L_{n-1})/2$ for $2 \leq i \leq n-1$, and $(L_n - L_{n-1})$ at $i = n$. Finally, a control method based on a relaxation factor, $r$, is implemented to minimize the numerical instabilities, reducing substantially the number of iterations to solve the equations system. This relaxation factor is introduced in Eq. (12) approximating the gas temperature as

$$T_{gas,TC_i} = \left[ \frac{\epsilon_{TC}\sigma}{h_{TC_i}} (T_s^4 - T_{TC}^4) + T_{TC} \right] r + T_{gas-1}[1 - r]. \tag{14}$$

The value of the relaxation factor, $r$, will determine the number of iterations required for the final temperature. Hence, the higher the relaxation factor is, the lower the number of iterations required and the greater the influence of the previous time step. At this point, Welch et al. [30] chose a value of 0.2 to 0.3, maintaining the number of iterations always lower than 10.

Applying this methodology in the tests described in this paper, a negligible influence ($<1\%$) has been observed in the thermocouples far from the fire plume. The thermocouples closer to flame are the ones in which the radiation influences more the measurements. Therefore, the higher the temperature of the thermocouples is, i.e. the higher HRRs, the greater uncertainty expected. Accordingly, the most affected thermocouple is the one closest to the flame, i.e. sensor 1 placed at 5.25 m height over the flame, and the average differences for this thermocouple are 9°C ($<2\%$), 18°C ($<3\%$), 24°C ($<6\%$) and 20°C ($<5\%$), in Test #1 to #4, respectively.

# Appendix 3: Experimental Data

See Tables 5, 6, 7 and 8.

**Table 5**
**Test #1. HRR = 1.7 MW. Asymmetric make-up air configuration. Steady extraction rate**

| Time (s) | Sensor 2 | Sensor 4 | Sensor 6 | Sensor 14 | Sensor 16 | Sensor 18 |
|---|---|---|---|---|---|---|
| 0 | 20 | 20 | 20 | 20 | 20 | 20 |
| 25 | 109 | 51 | 35 | 21 | 21 | 21 |
| 50 | 166 | 63 | 43 | 22 | 22 | 26 |
| 75 | 172 | 68 | 50 | 24 | 23 | 30 |
| 100 | 171 | 65 | 51 | 24 | 25 | 32 |
| 125 | 167 | 60 | 49 | 24 | 28 | 35 |
| 150 | 144 | 51 | 46 | 25 | 31 | 37 |
| 175 | 124 | 61 | 50 | 26 | 35 | 40 |
| 200 | 111 | 53 | 44 | 27 | 39 | 42 |
| 225 | 76 | 50 | 46 | 28 | 43 | 44 |
| 250 | 110 | 58 | 48 | 30 | 45 | 48 |
| 275 | 86 | 62 | 54 | 32 | 48 | 52 |
| 300 | 63 | 55 | 52 | 36 | 48 | 52 |
| 325 | 68 | 56 | 52 | 36 | 52 | 54 |
| 350 | 80 | 60 | 56 | 41 | 55 | 54 |
| 375 | 111 | 68 | 62 | 42 | 55 | 56 |

**Table 5**
**continued**

| Time (s) | Sensor 2 | Sensor 4 | Sensor 6 | Sensor 14 | Sensor 16 | Sensor 18 |
|---|---|---|---|---|---|---|
| 400 | 121 | 68 | 65 | 41 | 59 | 63 |
| 425 | 72 | 64 | 60 | 45 | 58 | 62 |
| 450 | 82 | 69 | 63 | 45 | 59 | 63 |
| 475 | 163 | 100 | 78 | 47 | 65 | 69 |
| 500 | 111 | 75 | 70 | 48 | 66 | 73 |
| 525 | 71 | 67 | 64 | 49 | 66 | 71 |
| 550 | 311 | 111 | 88 | 49 | 70 | 76 |
| 575 | 126 | 83 | 73 | 47 | 69 | 76 |
| 600 | 80 | 69 | 67 | 45 | 69 | 74 |
| 625 | 157 | 98 | 77 | 49 | 74 | 79 |
| 650 | 139 | 101 | 85 | 46 | 77 | 84 |
| 675 | 70 | 74 | 72 | 41 | 72 | 78 |
| 700 | 51 | 63 | 66 | 38 | 72 | 77 |

**Table 6**
**Test #2. HRR = 2.3 MW. Symmetric make-up air configuration.**
**Steady extraction rate**

| Time (s) | Sensor 2 | Sensor 4 | Sensor 6 | Sensor 14 | Sensor 16 | Sensor 18 |
|---|---|---|---|---|---|---|
| 0 | 18 | 18 | 18 | 18 | 18 | 18 |
| 25 | 201 | 74 | 46 | 20 | 20 | 21 |
| 50 | 229 | 86 | 54 | 22 | 21 | 28 |
| 75 | 283 | 92 | 59 | 24 | 24 | 34 |
| 100 | 286 | 89 | 58 | 26 | 29 | 40 |
| 125 | 316 | 109 | 64 | 27 | 35 | 44 |
| 150 | 332 | 117 | 74 | 28 | 39 | 48 |
| 175 | 301 | 109 | 74 | 31 | 44 | 51 |
| 200 | 314 | 115 | 75 | 33 | 48 | 56 |
| 225 | 292 | 112 | 80 | 34 | 52 | 58 |
| 250 | 283 | 110 | 79 | 35 | 55 | 62 |
| 275 | 321 | 113 | 82 | 36 | 58 | 64 |
| 300 | 335 | 125 | 89 | 38 | 61 | 67 |
| 325 | 284 | 124 | 88 | 39 | 64 | 70 |
| 350 | 321 | 119 | 90 | 38 | 66 | 72 |
| 375 | 300 | 114 | 87 | 39 | 69 | 74 |
| 400 | 310 | 118 | 89 | 40 | 70 | 76 |
| 425 | 336 | 121 | 94 | 39 | 73 | 79 |
| 450 | 246 | 115 | 95 | 41 | 75 | 79 |
| 475 | 319 | 117 | 93 | 42 | 78 | 81 |
| 500 | 260 | 122 | 95 | 43 | 80 | 83 |
| 525 | 265 | 128 | 97 | 41 | 80 | 83 |
| 550 | 263 | 121 | 98 | 42 | 80 | 84 |
| 575 | 251 | 127 | 96 | 40 | 81 | 85 |
| 600 | 255 | 120 | 100 | 43 | 81 | 86 |
| 625 | 258 | 120 | 100 | 44 | 83 | 86 |

**Table 7**
**Test #3. HRR = 3.9 MW. Symmetric make-up air configuration. Transient extraction rate**

| Time (s) | Sensor 2 | Sensor 4 | Sensor 6 | Sensor 14 | Sensor 16 | Sensor 18 |
|---|---|---|---|---|---|---|
| 0 | 21 | 21 | 21 | 21 | 21 | 21 |
| 25 | 297 | 84 | 46 | 25 | 25 | 27 |
| 50 | 377 | 111 | 65 | 29 | 28 | 38 |
| 75 | 486 | 126 | 75 | 32 | 39 | 48 |
| 100 | 467 | 123 | 77 | 33 | 48 | 59 |
| 125 | 501 | 133 | 82 | 36 | 56 | 65 |
| 150 | 477 | 132 | 89 | 39 | 64 | 70 |
| 175 | 433 | 136 | 96 | 41 | 73 | 77 |
| 200 | 464 | 153 | 107 | 44 | 76 | 82 |
| 225 | 453 | 145 | 110 | 47 | 80 | 89 |
| 250 | 470 | 163 | 115 | 53 | 84 | 92 |
| 275 | 422 | 154 | 115 | 56 | 90 | 98 |
| 300 | 427 | 147 | 116 | 56 | 93 | 101 |
| 325 | 478 | 164 | 122 | 58 | 97 | 106 |
| 350 | 480 | 152 | 123 | 57 | 102 | 109 |
| 375 | 472 | 149 | 122 | 60 | 104 | 112 |
| 400 | 389 | 146 | 118 | 58 | 107 | 112 |
| 425 | 409 | 144 | 117 | 53 | 108 | 113 |
| 450 | 349 | 124 | 114 | 51 | 109 | 112 |
| 475 | 405 | 131 | 112 | 49 | 110 | 112 |
| 500 | 344 | 111 | 103 | 48 | 111 | 112 |
| 525 | 405 | 129 | 107 | 46 | 109 | 110 |
| 550 | 400 | 138 | 112 | 47 | 109 | 108 |

**Table 8**
**Test #4. HRR = 5.3 MW. Symmetric make-up air configuration. Transient extraction rate**

| Time (s) | Sensor 2 | Sensor 4 | Sensor 6 | Sensor 14 | Sensor 16 | Sensor 18 |
|---|---|---|---|---|---|---|
| 0 | 17 | 17 | 17 | 17 | 17 | 17 |
| 25 | 323 | 90 | 62 | 23 | 21 | 26 |
| 50 | 434 | 132 | 72 | 27 | 30 | 39 |
| 75 | 298 | 128 | 86 | 32 | 48 | 52 |
| 100 | 506 | 142 | 90 | 35 | 59 | 64 |
| 125 | 518 | 159 | 104 | 39 | 65 | 72 |
| 150 | 472 | 169 | 124 | 43 | 75 | 82 |
| 175 | 378 | 159 | 122 | 52 | 85 | 89 |
| 200 | 445 | 170 | 127 | 61 | 92 | 101 |
| 225 | 265 | 147 | 129 | 71 | 100 | 108 |
| 250 | 374 | 157 | 137 | 84 | 106 | 116 |
| 275 | 267 | 155 | 138 | 87 | 114 | 125 |
| 300 | 206 | 146 | 135 | 84 | 117 | 129 |
| 325 | 374 | 169 | 144 | 75 | 122 | 128 |
| 350 | 246 | 149 | 136 | 66 | 125 | 134 |
| 375 | 309 | 147 | 135 | 59 | 129 | 135 |

**Table 8**
**continued**

| Time (s) | Sensor 2 | Sensor 4 | Sensor 6 | Sensor 14 | Sensor 16 | Sensor 18 |
|---|---|---|---|---|---|---|
| 400 | 485 | 180 | 143 | 57 | 130 | 135 |
| 425 | 451 | 178 | 149 | 55 | 131 | 136 |
| 450 | 497 | 188 | 151 | 56 | 132 | 134 |
| 475 | 545 | 205 | 161 | 56 | 132 | 136 |
| 500 | 519 | 207 | 147 | 60 | 133 | 136 |
| 525 | 494 | 169 | 145 | 59 | 132 | 135 |
| 550 | 510 | 185 | 148 | 58 | 133 | 134 |

# References

1. Floyd J, Forney G, Hostikk S, Korhonen T, McDermott R, McGrattan K (2013) Fire dynamics simulator (version 6). Technical reference guide, 1st edn. 1National Institute of Standard and Technology, Gaithersburg

2. NFPA92B (2005) Guide for smoke management systems in atria, covered malls, and large areas. National Fire Protection Association, Quincy

3. Chow WK, Yi L, Shi CL, Li YZ, Huo R (2005) Experimental studies on mechanical smoke exhaust system in an atrium. J Fire Sci 23(5):429–444

4. Lougheed GD, Hadjisophocleous GV, McCartney C, Taber BC (1999) Large-scale physical model studies for an atrium smoke exhaust system. ASHRAE Trans 105(1):1–23

5. Gutirrez-Montes C, Sanmiguel-Rojas E, Kaiser AS, Viedma A (2008) Numerical model and validation experiments of atrium enclosure fire in a new fire test facility. Build Environ 43(11):1912–1928. doi:10.1016/j.buildenv.2007.11.010

6. Gutirrez-Montes C, Sanmiguel-Rojas E, Viedma A, Rein G (2009) Experimental data and numerical modelling of 1.3 and 2.3 MW fires in a 20 m cubic atrium. Build Environ 44(9):1827–1839. doi:10.1016/j.buildenv.2008.12.010

7. Gutirrez-Montes C, Sanmiguel-Rojas E, Viedma A (2010) Influence of different make-up air configurations on the fire-induced conditions in an atrium. Build Environ 45(11):2458–2472. doi:10.1016/j.buildenv.2010.05.006

8. Gutirrez-Montes C, Sanmiguel-Rojas E, Burgos MA, Viedma A (2012) On the fluid dynamics of the make-up inlet air and the prediction of anomalous fire dynamics in a large-scale facility. Fire Saf J 51:27–41. doi:10.1016/j.firesaf.2012.02.007. http://www.sciencedirect.com/science/article/pii/S0379711212000331

9. McGrattan K (2004) Fire dynamics simulator (version 4) technical reference guide, 1st edn. 1National Institute of Standard and Technology, Gaithersburg

10. McGrattan K, Hostikka S, Floyd J, Baum H, Rehm R, Mell W, McDermott R (2008) Fire dynamics simulator (version 5). User's guide, 1st edn. 1National Institute of Standard and Technology, Gaithersburg

11. Klote JH (2008) The SFPE Handbook of Fire Protection Engineering, Section 4

12. Hadjisophocleous GV, Lougheed GD (1999) Experimental and numerical study of smoke conditions in an atrium with mechanical exhaust. Int J Eng Perform-Based Fire Codes 1(3):183–187

13. Yi L, Chow WK, Li YZ, Huo R (2005) A simple two-layer zone model on mechanical exhaust in an atrium. Build Environ 40(7):869–880

14. Kerber S, Milke J (2007) Using FDS to simulate smoke layer interface height in a simple atrium. Fire Technol 43(1):45–75. doi:10.1007/s10694-007-0007-7

15. Hadjisophocleous G, Zhou JJ (2008) Evaluation of atrium smoke exhaust make-up air velocity. ASHRAE Trans 114(1):147–155

16. Lougheed GD, Hadjisophocleous GV (1997) Investigation of atrium smoke exhaust effectiveness. ASHRAE Trans 103(2):519–533

17. Kashef A, Benichou N, Lougheed G, McCartney C (2002) A computational and experimental study of fire growth and smoke movement in large spaces. In: Proceedings of 10th Annual Conference of the CFD Society of Canada (CFD 2002), vol. 40, pp. 466–471

18. Cooper LY, Harkleroad M, Quintiere J, Rinkinen W (1982) An experimental study of upper hot layer stratification in full-scale multiroom fire scenarios. J Heat Transf 104(4):741–749. doi:10.1115/1.3245194

19. Quintiere JG, Steckler K, Corley D (1984) An assessment of fire induced flows in compartments. Fire Sci Technol 4(1):1–14. doi:10.3210/fst.4.1

20. Emmons HW (2003) The SFPE handbook of fire protection engineering, Chap 2–3: Vent flows, 3rd edn. National Fire Protection Association Quincy, Massachusetts

21. Janssens M, Tran HC (1992) Data reduction of room tests for zone model validation. J Fire Sci 10(6):528–555. doi:10.1177/073490419201000604. http://jfs.sagepub.com/content/10/6/528

22. He Y, Fernando A, Luo M (1998) Determination of interface height from measured parameter profile in enclosure fire experiment. Fire Saf J 31(1):19–38. doi:10.1016/S0379-7112(97)00064-7. http://www.sciencedirect.com/science/article/pii/S0379711297000647

23. Ayala P, Cantizano A, Gutirrez-Montes C, Rein G (2013) Influence of atrium roof geometries on the numerical predictions of fire tests under natural ventilation conditions. Energy Build 65:382–390. doi:10.1016/j.enbuild.2013.06.010. http://www.sciencedirect.com/science/article/pii/S0378778813003484

24. SFPE (2002) Handbook of fire protection engineering, 3rd edn. National Fire Protection Association, Quincy

25. Hill K, Dreisbach J, Joglar F, Najafi B, McGrattan K, Peacock R, Hamins A (2007) Verification and validation of selected fire models for nuclear power plant applications. Tech. Rep. NUREG 1824, United States Nuclear Regulatory Commission, Washington, DC

26. Hostikka S, Kokkala M, Vaari J (2001) Experimental study of the localized room fires. NFSC2 Test Series, VTT Research Notes 2104. Finland, Technical Research Centre of Finland

27. Beji T, Verstockt S, Van de Walle R, Merci B (2012) Prediction of smoke filling in large volumes by means of data assimilation-based numerical simulations. J Fire Sci 30(4):300. doi:10.1177/0734904112437845. http://jfs.sagepub.com/content/30/4/300.abstract

28. Tilley N, Merci B (2009) Application of FDS to adhered spill plumes in atria. Fire Technol 45(2):179–188. doi:10.1007/s10694-008-0079-z

29. Blevins LG, Pitts WM (1999) Modeling of bare and aspirated thermocouples in compartment fires. Fire Saf J 33(4):239–259. doi:10.1016/S0379-7112(99)00034-X. http://www.sciencedirect.com/science/article/pii/S037971129900034X

30. Welch S, Jowsey A, Deeny S, Morgan R, Torero JL (2007) BRE large compartment fire tests—characterising post-flashover fires for model validation. Fire Saf J 42(8):548–567. doi:10.1016/j.firesaf.2007.04.002. http://www.sciencedirect.com/science/article/pii/S0379711207000343

31. NIST/SEMATECH (2010) e-Handbook of Statistical Methods. http://www.itl.nist.gov/div898/handbook/S

32. Smits AJ, Dussauge J-P (2010) Turbulent shear layers in supersonic flow, 2nd edn. Springer, New York